Synthesis of tungsten carbide on Al-SBA-15 mesoporous materials by carburization

M.G. Alvarez[a], R.J Chimentao[a,f,*], D. Tichit[b], J.B.O. Santos[c], A. Dafinov[a], L.B. Modesto-Lopez[a,e], J. Rosell-Llompart[a,d], E.J. Güell[a], F. Gispert-Guirado[a], J. Llorca[g], F. Medina[a]

[a] Department of Chemical Engineering, Universitat Rovira i Virgili Campus Sescelades, 43007 Tarragona, Spain
[b] Institut Charles Gerhardt, Equipe Matèriaux Avancès pour la Catalyse et la Santè, 34296 Montpellier Cedex 5, France
[c] Universidade Federal de Sa-o Carlos, Sa-o Carlos, Brazil
[e] Department of Aerospace Engineering and Fluid Mechanics, University of Seville, Sevilla, Spain
[d] Catalan Institution for Research and Advanced Studies (ICREA), Barcelona, Spain
[f] School of Chemistry, Yachay Tech, Yachay City of Knowledge, Urcuqui, Ecuador
[g] Universitat Politècnica de Catalunya, Barcelona, Spain

Keywords:
Tungsten carbide
Mesoporous silica
SBA-15
Al-SBA-15

a b s t r a c t

Aluminum was incorporated into SBA-15 supports at molar ratios Si/Al ¼ 10 and 2 by the pH-adjusting method. The calcined mesoporous Al-SBA-15 supports, as well as the Al-free SBA-15 support, were impregnated with ammonium paratungstate ($(NH_4)_{10}[H_2W_{12}O_{42}]4H_2O$) aqueous solution. Tungsten carbide (W_2C) was synthesized by temperature programmed carburization (TPC) from the WO_3 supported on Al-SBA-15 and SBA-15 in a flow of CH_4/H_2. These resultant materials were characterized by powder X-ray diffraction (XRD), N_2 adsorption/desorption, ^{27}Al NMR and Raman spectroscopies, and transmission electron microscopies (TEM and HRTEM). W_2C species were obtained after the carburization process in all the materials. The mesoporous structure of the SBA-15 supports was preserved at all synthesis steps. XRD and TEM analyses revealed that the introduction of aluminum species into the SBA-15 greatly enhanced the dispersion of WO_3 and W_2C phases during the calcination and carburization steps, respectively. In situ XRD measured during the carburization in a synchrotron facility provided further details of the reduction of tungsten trioxide species as a function of temperature. The presence of aluminum in the SBA-15 notably affected the distribution and the reduction temperature of the tungsten oxide species.

1. Introduction

The discovery of ordered mesoporous silicates SBA-15 provided a versatile potential for the design of new materials [1]. SBA-15 is formed of highly uniform arrays of hexagonal tubular channels of amorphous SiO_2, with pore diameter in the 5e30 nm range [2]. The ordered mesoporous structure, large surface area and remarkable hydrothermal stability of the SBA-15 [3] offer an attractive opportunity for the synthesis of supported tungsten carbides within the mesoporous silica channels.

Transition metal carbides, especially tungsten carbide, are appreciated in industrial applications, such as machine tool coatings, for their high hardness, wear resistance, high melting point and chemical inertness [4]. The transition metal carbides have comparable catalytic performance to noble metals, as pointed out by the pioneering work of Volpe and Boudart [5]. Such catalytic behavior has been demonstrated in hydrodesulfurization (HDS) of oil and gas [6], hydrocarbon isomerization [7] and CH_4 reforming to synthesis gas [8].

The synthesis of carbides is usually performed by temperature programmed carburization (TPC) of an oxide precursor using CH_4 as carbiding agent in a mixture with H_2 [9]. The carburization is a complex reaction in which a mixture of different tungsten carbide phases such as WC_{1-x}, W_2C and WC is formed [10]. The structure of the material which supports the oxide precursor can markedly

* Corresponding author.School of Chemistry, Yachay Tech, City of Knowledge, Urcuqui, Ecuador.
E-mail address: rchimenton@yachaytech.edu.ec (R.J. Chimentao).

influence the formed metal species [11,12]. Transition metal carbides suffer strong sintering on conventional Al_2O_3 and SiO_2 supports under the TPC process [13]. However, sintering is minimized when tungsten carbides are formed on SBA-15, presumably by the confinement of the metal precursor species within the SBA-15 channels [14].

The incorporation of a heteroatom into the SBA-15 structure is known to affect the interaction between the tungsten species and the SBA-15 support. It may also enhance the mechanical and chemical resistance of the resulting mesoporous silica-based material [15-18]. Among a large number of possible heteroatoms that can be substituted in silicate structures, Al is most favorable from the point of view of generating Brønsted acidity, which is a required property in many industrial reactions [19-21]. Direct-synthesis and post-synthesis grafting are two typical methods used for the introduction of heteroatoms in mesoporous silica materials [22]. Wu et al. [22] introduced Al and Ti into SBA-15 by the pH-adjusting method in strong acid media, followed by a hydrothermal treatment.

The synthesis of tungsten carbide into SBA-15 has been reported in the literature [23]. However, the effect of incorporating Al into the SBA-15 structure on the synthesis of tungsten carbides has not been previously studied. Herein, we report a detailed study of the carburization of tungsten oxides supported on SBA-15 and Al-SBA-15 materials. The Al-SBA-15 supports were synthesized by the pH-adjusting method. The tungsten oxide precursor was obtained by calcination of the SBA-15 supports impregnated with an aqueous solution of ammonium paratungstate. Finally, the carburization of the tungsten oxide precursors was performed. The scopes of this work are the study on how the synthesis of tungsten carbide may affect the structural integrity of the SBA-15 and how the presence of aluminum in SBA-15 can affect the reduction of the tungsten oxide precursor.

2. Experimental

2.1. Synthesis of siliceous SBA-15

The mesoporous silica SBA-15 was synthesized under acid conditions using triblock copolymer P123 poly(ethylene oxide)/poly(propylene oxide)/poly-(ethylene oxide), ($EO_{20}PO_{70}EO_{20}$), as a template [2,24]. Typically, 4 g of P123 was dissolved in a solution of 100 mL of distilled water acidulated with 25 mL of HCl (37%, Sigma–Aldrich). The resultant mixture was stirred for 2 h at 328 K. Finally 9.45 g of tetraethoxysilane (TEOS) was added to the mixture under stirring. The gel composition P123:HCl:H_2O:TEOS was 0.017:5.88:197:1 in molar ratio. The resulting mixture was stirred at 328 K for 5 h and then transferred into a Teflon-lined stainless steel autoclave and aged at 403 K for 24 h.

After cooling down to room temperature, the product was filtered, washed with distilled water and dried overnight at 333 K. The sample was then calcined in a muffle furnace in static atmosphere at 823 K (heating rate 2 K/min) for 8 h to remove the copolymer template.

2.2. Synthesis of Al-SBA-15

Al-SBA-15 samples were prepared by the pH-adjusting method described by Wu et al. [22] as follows: 0.781 g of P123 was dissolved in 25 mL of HCl 2 M. Once dissolved the P123, 1.71 g of TEOS was added drop wise to the solution. The mixture was stirred for 4 h followed by the addition of $Al(NO_3)_3\$9H_2O$ to reach Si/Al molar ratios in solution of 2 and 10. The mixtures were stirred during 4 h and then transferred into a Teflon-lined stainless steel autoclave for further condensation of the silica species at 373 K for 48 h.

After this procedure, the pH of the mixture was adjusted to 7.5 by drop wise addition of a 1 M NaOH aqueous solution. The mixture was kept in hydrothermal treatment at 373 K for 48 h [22]. Then, the product was filtered, washed with distilled water and dried overnight at 333 K. The sample was then calcined at 723 K (heating rate 2 K/min) for 8 h to remove the copolymer template.

2.3. Synthesis of the supported carbides

Firstly, SBA-15, Al-SBA-15 (Si/Al ¼ 2) and Al-SBA-15 (Si/Al ¼ 10) were impregnated with an aqueous solution of ammonium paratungstate ($(NH_4)_{10}\$[H_2W_{12}O_{42}]\$4H_2O$) to obtain 30 wt.% of tungsten oxide (WO_3). The SBA-15 and Al-SBA-15 supports were previously calcined at 473 K for 2 h. After impregnation the samples were dried at 393 K for 12 h and calcined at 723 K in a muffle furnace in static atmosphere for 4 h. The impregnated samples were denoted by WO_3/SBA-15, WO_3/Al-SBA-15 (Si/Al ¼ 2) and WO_3/Al-SBA-15 (Si/Al ¼ 10).

Tungsten carbide was prepared by temperature programmed carburization (TPC) of WO_3 containing samples in a flow of CH_4/H_2 (20/80 v/v). The TPC was carried out in a quartz fixed bed down reactor with controlled flow. The temperature was raised from room temperature to 973 K at the rate of 5 K/min and kept at 973 K for 5 h. The reactor temperature was monitored by thermocouple inserted into the fixed bed connected to the thermo-controller. After cooling, the tungsten carbides samples were passivated by 1% O_2/Ar (v/v). The tungsten carbides samples were denoted by W_2C/SBA-15, W_2C/Al-SBA-15 (Si/Al ¼ 2) and W_2C/Al-SBA-15 (Si/Al ¼ 10).

2.4. Characterization

Si, Al and W chemical analyses were obtained by induced coupled plasma (ICP-OES) using an Optima 8x00 Perkin Elmer instrument after microwave decomposition of the samples in a mixture of HCl:HF:H_2O with a volume ratio of 5:1:3, respectively.

Specific surface areas were determined by nitrogen adsorption at 77 K using a Micromeritics ASAP 2020 equipment. Samples were previously degassed in situ at 523 K under vacuum. Surface areas were calculated using the Brunauer–Emmet–Teller (BET) method and Barrett–Joyner–Halenda (BJH) pore size distribution was calculated from the desorption branch.

The ^{27}Al NMR spectra were recorded on a Bruker Varian Mercury VX-400 spectrometer at room temperature using a 7 mm probe and $AlCl_3\$6H_2O$ was used as a reference.

Raman spectra of the samples were obtained by using a T64000 Jobin Ivon spectrometer. Approximately, 10 mg of each sample was excited using an Ar laser operating at 785 nm and a power of 2 mW.

Selected samples were analyzed by transmission electron microscopy (TEM) using a JEOL JEM-2100 instrument at an accelerating voltage of 100 kV. The samples were prepared by dispersing the as-prepared catalysts in ethanol and then drop casting the suspension on a standard 3 mm holey carbon-coated copper grid and letting the ethanol evaporate at room temperature.

High-resolution transmission electron microscopy (HRTEM) was carried out with a JEOL 2010F instrument equipped with a field emission source. The point-to-point resolution was 0.19 nm and the resolution between lines was 0.14 nm.

The XRD patterns of the materials were recorded using a Siemens D5000 diffractometer (Bragg–Brentano for focusing geometry and vertical θ–θ goniometer) with an angular 2θ-diffraction in the 0.5°-5° and 5°-90° ranges. The passivated samples were dispersed on a Si(510) low background sample holder. Diffractograms were collected with an angular step of 0.03° at 5 s per step.

Cu Kα radiation (λ ¼ 1.54 Å) was obtained from a copper X-ray tube operated at 40 kV and 30 mA.

The in situ XRD measurements of the reduction in a flow of CH_4/H_2 (20/80 v/v) were performed at the ESRF synchrotron (BM25A SpLine, Grenoble, France). Approximately 100 mg of WO_3 containing sample (WO_3/SBA-15 and WO_3/Al-SBA-15 (Si/Al ¼ 10)) was hand pressed into a thin pellet (approximately 1.0 cm in diameter and 0.25 cm in thickness). The pellet sample was then placed in a cell reactor to be analyzed in transmission mode (2 × 2 mm^2 approximate beam size). This cell reactor was an HPHT (high pressure high temperature) cell from SPECAC Brillant Spectroscopy provided with Kapton™ windows. A 50 std. mL/min total gas flow of the 20/80 v/v CH_4/H_2 mixture was set by a Brooks 0152 flow controller. During in situ XRD the sample was heated from room temperature to 885 K at the rate of 5 K/min, and then kept at 885 K for 70 min. The sample was then cooled in Ar purge flow to room temperature. The diffracted X-rays were recorded on a CCD detector charge-coupled device, MarCCD 133 with (49.2 × 49.2) mm^2 sensitive area and four amplifiers selected for low noise (4e6 e^- RMS) placed 34 cm away from the sample, for an X-ray wavelength of 0.6199 Å (20 keV) and Bragg angle range of 2θ ¼ 2.2°e22°. The exposure time for the CCD detector was 300 s typically, and ca. 70 scans were acquired in one experiment. The CCD was calibrated with a reference sample of α-Al_2O_3 (SRM 676). Each CCD image was converted to conventional 2θ-diffractograms by azimuthal integration (X-ray Oriented Programs, XOP 2.3 Software). Subsequent treatment for quantification of the crystalline phases was performed by the Rietveld method by using TOPAS 4.2 software.

3. Results and discussion

3.1. Chemical composition

The Si/Al molar ratios of the two Al-SBA-15 materials and W content in the supported trioxide samples were determined by ICP-OES. The Si/Al ratios were consistent with the concentrations in the starting solutions (Table 1), while the tungsten concentrations were slightly lower than the nominal value of 23.8 wt.%.

3.2. Textural properties

Isotherms of N_2 adsorptionedesorption of all SBA-15 samples are shown in Fig. 1. All SBA-15 samples display a typical type IV isotherm with an H1 type hysteresis loop. This kind of adsorption is characteristic of mesoporous materials with 2D-hexagonal structure [3].

After introduction of Al and W species, the type IV isotherm as well as the narrow pore size distributions was still preserved, as shown in Fig. 1a and b, respectively. Some differences among these samples can be envisaged. For instance, SBA-15 and Al-SBA-15 (Si/Al ¼ 10) (Fig. 1a) presented a steep jump at relatively high partial pressure ($P/P_0 \geq 0.7$), while Al-SBA-15 (Si/Al ¼ 2) presented a broader jump at lower relative pressure ($P/P_0 \geq 0.45$).

An effect of Al incorporated into SBA-15 on the textural properties, i.e. specific surface areas (S_{BET}), pore volumes (V_P), pore diameters (d_P) and pore size distributions can be distinguished (Table 1 and inset of Fig. 1a). Similar S_{BET} and V_P were obtained for both SBA-15 and Al-SBA-15 (Si/Al ¼ 10) materials, while d_P for Al-SBA-15 (Si/Al ¼ 2) was higher than for SBA-15. These results are in agreement with those obtained by Yue et al. [25]. However, the S_{BET} and V_P decreased by about 33% and 40%, respectively, in the sample with higher Al content (Al-SBA-15 (Si/Al ¼ 2)) relative to the corresponding Al-free sample (Table 1). A smaller d_P was determined for Al-SBA-15 (Si/Al ¼ 2) than for Al-SBA-15 (Si/Al ¼ 10). Studies on post synthesis alumination of SBA-15 in basic media reported by Kao et al. [24] indicated a decrease in surface area with the increase of aluminum content which was attributed to the alkaline dissolution of the structure. Since both kinds of Al-incorporated SBA-15 samples of this study were prepared by the same protocol steps than Kao et al. [24] we could not discard the formation of segregated aluminum-containing phases. Indeed, ^{27}Al solid state NMR performed on Al-SBA-15 (Si/Al ¼ 2) revealed the presence of extra-framework alumina (vide infra).

The calcination at 723 K of the impregnated SBA-15 and Al-SBA-15 materials with ammonium paratungstate resulted in a decrease of S_{BET} and V_P compared with the corresponding calcined bare supports (Fig. 1b, Table 1). This may indicate a partial filling of the pores by tungsten oxides during calcination. Similar results were found by Wu et al. [22] during preparation of tungsten carbide confined in the channels of SBA-15.

A decrease in S_{BET} was also observed after carburization of WO_3 supported on SBA-15 and Al-SBA-15 (Fig. 1c, Table 1). This is consistent with the presence of tungsten carbide species both inside and on the walls of the channels of SBA-15, as observed by TEM images (vide infra W_2C/SBA-15 sample). During the carburization process the blocking of pores cannot be ruled out, which would explain the significant reduction in surface area observed, particularly for the W_2C/Al-SBA-15 (Si/Al ¼ 2) material (Table 1) when compared with the bare SBA-15 support.

The pore size distributions of the WO_3-containing samples and of their corresponding supported carbides samples are shown in the insets of Fig. 1b and c, respectively. The d_P values of the WO_3/Al-SBA-15 materials (Si/Al ¼ 10 and Si/Al ¼ 2) revealed a decrease when compared with the bare Al-SBA-15 supports (Table 1). Likewise, the d_P values for the W_2C/Al-SBA-15 samples were lower than those for the corresponding WO_3/Al-SBA-15 supports. Similarly, but more slightly, d_P of the SBA-15 decreased from 7.84 to 7.63 nm after impregnation with ammonium paratungstate and

Table 1
Chemical analysis and textural and structural parameters of the SBA-15-based materials.

Sample	N_2 adsorptionedesorption			XRD analysis		ICP	
	S_{BET} (m^2/g)	V_P (cm^3/g)	d_{pore} (nm)	a[a] (nm)	w[b] (nm)	Si/Al	W (wt.%)
SBA-15	541	0.98	7.84	11.26	3.6	e	e
Al-SBA-15 (Si/Al ¼ 10)	540	0.90	9.42	11.55	2.1	11.2	e
Al-SBA-15 (Si/Al ¼ 2)	364	0.60	7.71	11.19	3.5	2.5	e
WO_3/SBA-15	347	0.66	7.63	11.05	3.4	e	17.9
WO_3/Al-SBA-15 (Si/Al ¼ 10)	304	0.62	7.59	11.11	3.5	e	16.2
WO_3/Al-SBA-15 (Si/Al ¼ 2)	281	0.44	5.29	10.78	5.5	e	20.4
W_2C/SBA-15	272	0.54	7.46	11.13	3.7	e	e
W_2C/Al-SBA-15 (Si/Al ¼ 10)	234	0.29	4.71	11.10	6.4	e	e
W_2C/Al-SBA-15 (Si/Al ¼ 2)	189	0.28	4.60	10.94	6.3	e	e

[a] XRD unit-cell parameter a ¼ $2d_{100}/\sqrt{3}$.
[b] Wall thickness, w ¼ a − d_{pore}.

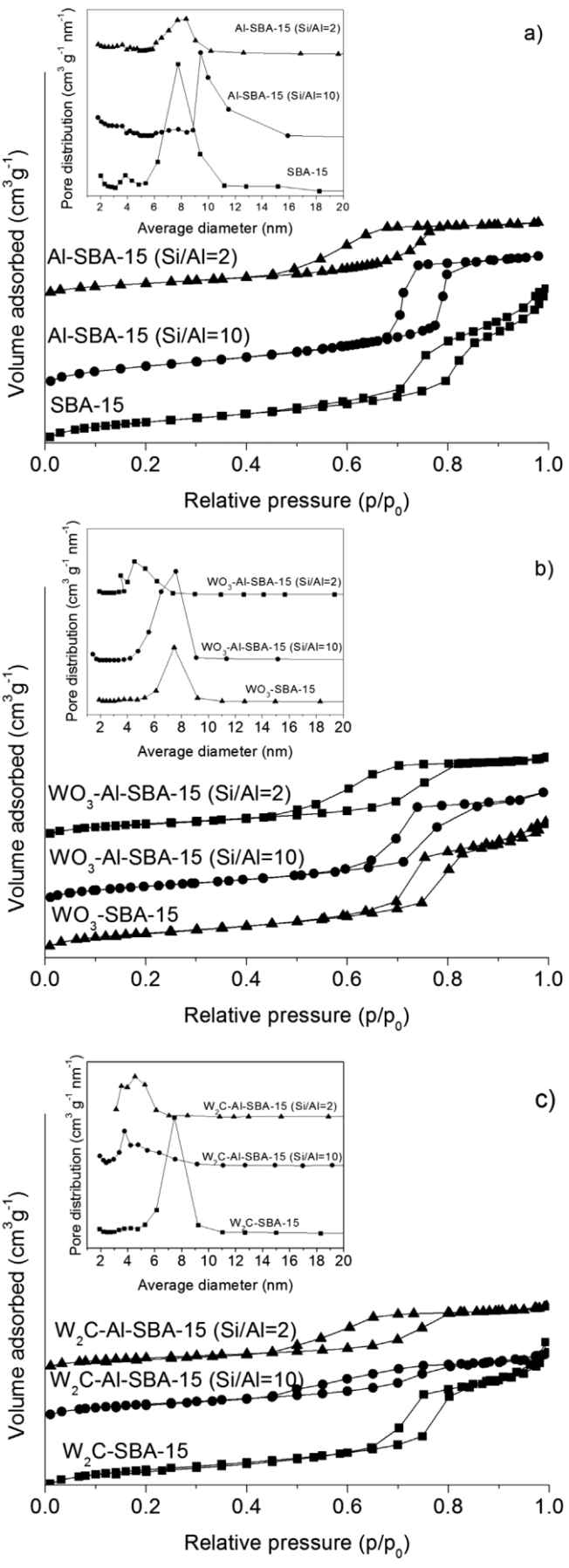

Fig. 1. Nitrogen adsorptionedesorption isotherms at 77 K: (a) as-synthesized Al-SBA-15 samples; (b) tungsten oxides supported (Al)-SBA-15 samples; (c) tungsten carbide supported Al-SBA-15 samples. Insets: corresponding pore size distribution.

calcination and further to 7.46 nm after carburization. Therefore, it can be seen that d_P was affected after each preparation step of tungsten carbides; however, the mesoporous structure of SBA-15 was preserved without noticeable modifications in the mesoscopic ordering.

3.3. Structural features

The low 2q angle XRD patterns of the SBA-15 and Al-SBA-15 (Si/Al ¼ 10 and Si/Al ¼ 2) materials showed three reflections indexed to (100), (110), and (200) of a hexagonal phase (inset in Fig. 2a). The presence of these peaks suggests that the characteristic hexagonal feature of the parent SBA-15 was preserved in all samples. Previous works reported that the unit-cell parameter (a) of the Al-containing mesoporous silica materials generally increases with the amount of aluminum introduced [26e28]. This is due to the longer AleO bond length compared to the SieO bond length. In our samples, the unit-cell parameter increased from 11.26 nm for SBA-15 to 11.55 nm for Al-SBA-15 (Si/Al ¼ 10). However, this trend reversed when the Al content was further increased to reach a Si/Al molar ratio of 2, where a slightly smaller a unit-cell parameter (11.19 nm) is observed. This is in agreement with the formation of additional phases of aluminum which could not be detected by XRD. The XRD peaks at the low 2q range of Al-SBA-15 (Si/Al ¼ 10) and Al-SBA-15 (Si/Al ¼ 2) materials were more intense than those of SBA-15 parent material, indicating higher structural organization (inset Fig. 2a).

The XRD patterns at low 2q angle range of the WO_3/SBA-15 and WO_3/Al-SBA-15 samples (inset Fig. 2b) revealed the characteristic peaks of the two dimensional hexagonal cell of the silica support. The low-angle XRD patterns of the W_2C/SBA-15 and W_2C/Al-SBA-15 samples (inset Fig. 2c) also revealed the preservation of the mesoporous structure. In addition, the 100 planes progressively shifted to higher 2q angles after the impregnation, calcination and carburization steps, accompanied by a decrease in the cell parameter a. Both of these effects are consistent with the reduction of the pore diameters observed by N_2-physisorption (Table 1).

The high 2q angle XRD patterns of the SBA-15 and Al-SBA-15 parent materials showed the presence of broad peaks attributed to amorphous silica phase (Fig. 2a). On the other hand, the high 2q angle XRD patterns of the supported tungsten oxide samples revealed diffraction peaks at 23.08°, 23.58°, 24.26°, 26.54°, 28.75°, 33.28° and 41.66° 2q angles, characteristic of monoclinic tungsten trioxide phase (WO_3, $P2_1/n$ space group) (Fig. 2b). These peaks become weaker in WO_3/Al-SBA-15 (Si/Al ¼ 10) and even disappear in WO_3/Al-SBA-15 (Si/Al ¼ 2). This suggests that the WO_3 particles were highly dispersed and the degree of dispersion greatly depended on the amount of Al contained in the support, or that the crystalline phase did not form. However, this last hypothesis is less likely considering the decrease of surface areas and pore sizes after impregnation with tungsten oxide species.

In attempting to rationalize this marked effect on the dispersion of the WO_3 species by the presence of aluminum in the SBA-15 support, the dispersion capability of tungsten cations on metal oxides can be considered. XPS studies on WO_3eAl_2O_3 by Iglesia et al. [29] provide an estimation of the maximum planar packing density of WO_3 species as 3.7 W^{b6} nm^{-2}. Other works [30] on WO_3eSiO_2 systems have reported a dispersion capability of WO_3 on mesoporous silica of only 0.5 W^{b6} nm^{-2}. Our data suggest that the interaction of tungsten oxide with pure silica may be weaker than that of tungsten oxide with aluminum-containing silica, in

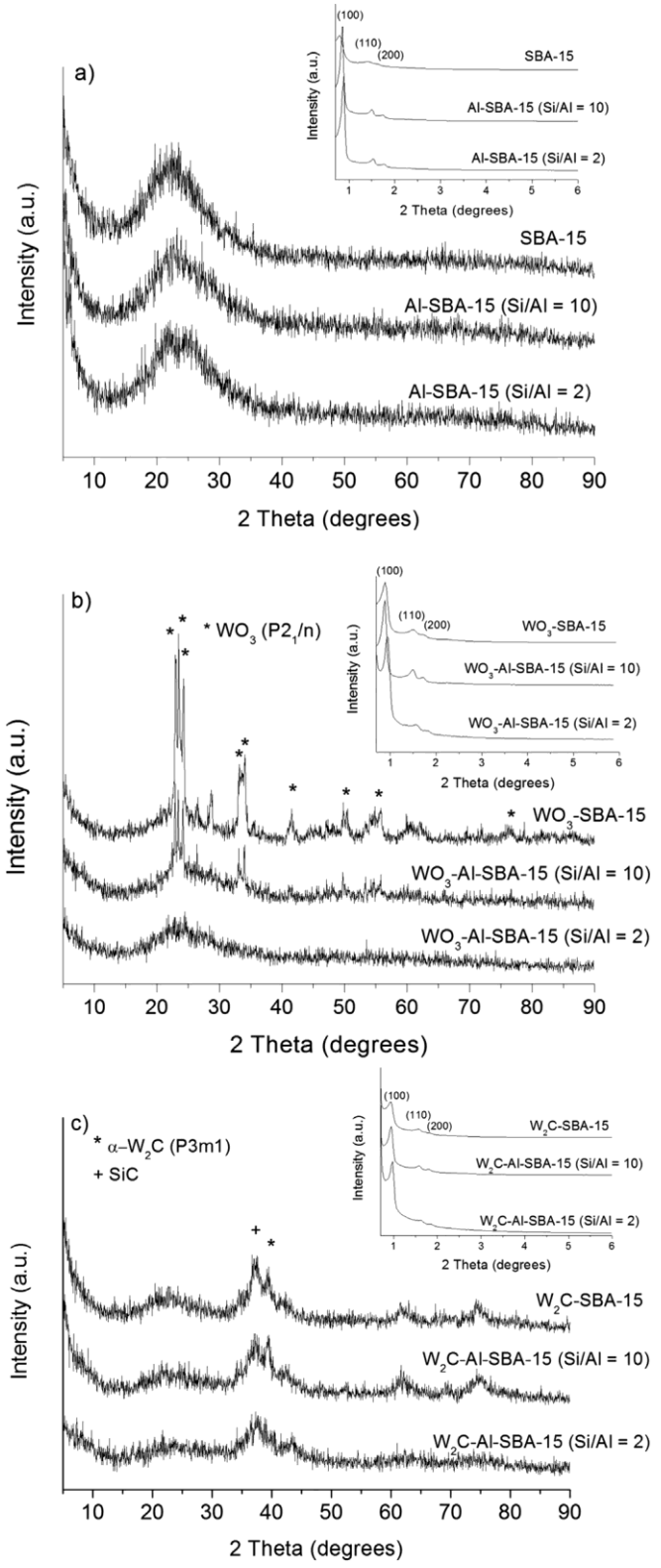

Fig. 2. High 2θ angle PXRD patterns of SBA-15 materials: (a) as-synthesized Al-SBA-15 samples; (b) tungsten oxides supported Al-SBA-15 samples; (c) tungsten carbide supported (Al)-SBA-15 samples. Insets: Low 2θ angle PXRD patterns of the corresponding materials.

agreement with the above mentioned works [29,30]. Here, this different interaction was indeed mirrored by the different dispersion of the tungsten oxide species on the Al-free and Al-containing silica supports, as suggested by the XRD and Raman analyses (vide infra, Fig. 4).

For the samples after carburization, the XRD patterns at high 2θ range revealed the characteristic peaks of α-W_2C (P3m1, ICDD: 35-776) which are identified at 34.34°, 37.84°, 39.35°, 61.59° and 74.69° (Fig. 2c) as well as a peak at 35.5° corresponding to SiC. In addition, larger pore wall thicknesses (w) were observed in the tungsten trioxide and carbide supported on aluminum-containing silica materials when compared to their corresponding bare supports, as shown in Table 1. This is consistent with the lower specific surface areas and pore volumes observed for the SBA-15 materials containing Al and W species by physisorption (Table 1).

3.4. ^{27}Al solid state NMR characterization

^{27}Al NMR can give valuable information on how the aluminum has been incorporated to the SBA-15 structure. Usually, tetra- and octa-coordinated Al species are present in mesoporous aluminosilicate materials [31]. Notably, the sample with lower aluminum content (Al-SBA-15 (Si/Al ¼ 10), Fig. 3 top) has nearly 100% tetrahedral Al (z57 ppm). However, sample Al-SBA-15 (Si/Al ¼ 2) (Fig. 3 bottom) also presented a signal at about 3 ppm corresponding to octahedral Al. Therefore, a large amount of Al species must have been introduced into the SBA-15 by the pH-adjusting method and,

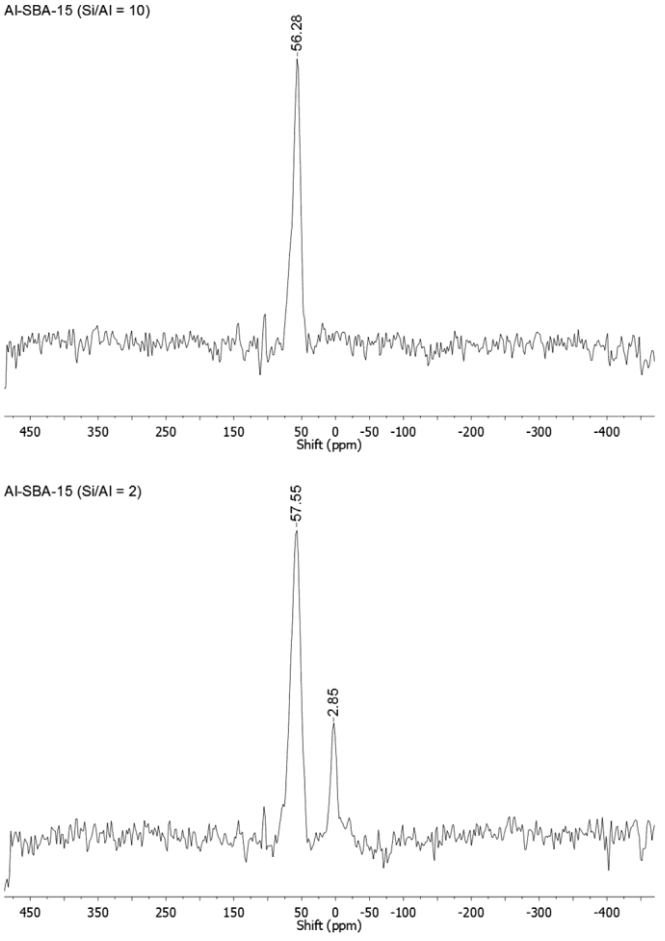

Fig. 3. ^{27}Al NMR spectra of samples Al-SBA-15 (Si/Al ¼ 10) (top) and Al-SBA-15 (Si/Al ¼ 2) (bottom).

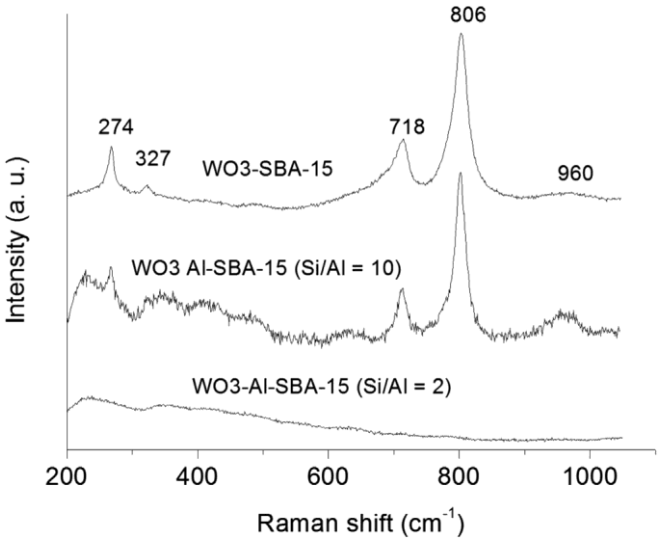

Fig. 4. RAMAN spectra of WO_3/SBA-15 and WO_3/Al-SBA-15 (Si/Al ¼ 10 and Si/Al ¼ 2, respectively) samples.

furthermore, the Al species introduced belong to the silicoaluminate structure. However, when higher amount of Al was introduced in Al-SBA-15 (Si/Al ¼ 2), some octahedral aluminum species were formed. The presence of this extra-framework aluminum in Al-SBA-15 (Si/Al ¼ 2) may be the cause of the slightly different textural and structural features discussed above.

3.5. Raman spectroscopy

Structural information of the metal oxides can be provided by Raman spectroscopy. The Raman vibrational modes are determined by the symmetry and structure of the coordinated compound [32]. Fig. 4 shows the Raman spectrum of the WO_3/SBA-15 and WO_3/Al-SBA-15 (Si/Al ¼ 10 and Si/Al ¼ 2) samples.

The Raman spectrum of the WO_3/SBA-15 sample (Fig. 4) shows major bands at about 274 cm^{-1}, 327 cm^{-1}, 718 cm^{-1}, and 806 cm^{-1}. These are characteristic of octahedrally coordinated tungsten oxide species. The Raman peak at 274 cm^{-1} is associated to WeO bending modes of monoclinic WO_3. The peak at 327 cm^{-1} is assigned to the bending vibration d(OeWeO) [33]. A band at ~960 cm^{-1} is also observed, which is characteristic of tetrahedrally coordinated tungsten oxide species. This band notably increases its relative intensity (with respect to bands at 806 and 718 cm^{-1}) upon introduction of Al into the SBA-15. Kuzmin et al. [34] attribute the presence of this band to surface tungsten-oxygen bonds, which increase in number when decreasing the particle size. This interpretation requires that the dispersion of the tungsten species on WO_3/SBA-15 sample be lower than that observed on WO_3/Al-SBA-15 (Si/Al ¼ 10), which is a scenario in agreement with our XRD results.

The Raman spectra for the WO_3/Al-SBA-15 (Si/Al ¼ 2) (Fig. 4) material revealed that no bulk WO_3 species are present.

3.6. In situ XRD analysis

Tungsten oxide reduces to tungsten carbide species (WC) under CH_4/H_2 atmosphere in the stepwise sequence of WO_3 $WO_{2.92}$ $WO_{2.66}$ WO_2 W_2C WC [35]. Here, we particularly followed the reduction steps of the tungsten oxide precursor by in situ XRD under CH_4/H_2 atmosphere.

Fig. 5a and b displays the in situ XRD patterns recorded during the reduction of the supported monoclinic tungsten trioxide ($P2_1/n$) on SBA-15 and Al-SBA-15 (Si/Al ¼ 10), respectively. The contribution of the different tungsten oxide phases present in each sample during the reduction was quantified by the Rietveld method (Fig. 5cef).

Fig. 5a and c shows that up to about 600 K the monoclinic WO_3 phase ($P2_1/n$, ICDD: 83-950) [36] present in WO_3/SBA-15 did not change. Above 600 K, orthorhombic WO_3 phase (Pcnb, ICDD: 89-4480) [37] was formed at the expense of the monoclinic WO_3 phase. Indeed, these two WO_3 phases coexisted in the temperature range from 600 K to 780 K.

Above 700 K, two additional tungsten oxide phases appeared, increasing until 820 K. The first one of these phases, which appeared at around 730 K, was attributed to tetragonal WO_3 (P4/ncc, ICDD: 88-366) [38]. The second one, which appeared close to 780 K, was ascribed to $WO_{2.92}$ (P2/c, ICDD: 71-0070) [39]. The monoclinic and the orthorhombic tungsten trioxide phases disappeared respectively at 780 and 830 K. Therefore, the sequence observed in the reduction process of WO_3/SBA-15 is: WO_3 ($P2_1/n$) WO_3 (Pcnb) WO_3 (P4/ncc) $WO_{2.92}$ (P2/c). Some of these phases coexisted in a large range of temperature. The amount of each tungsten oxide phase as a function of the reduction temper- ature determined by Rietveld method is presented in Fig. 5c. After keeping the sample at 885 K for 70 min, WO_3/SBA-15 contains 44 wt.% of WO_3 (P4/ncc) and 56 wt.% of $WO_{2.92}$ (P2/c) species (Fig. 5e).

The presence of aluminum in the WO_3/Al-SBA-15 (Si/Al ¼ 10) (Fig. 5b) support caused an increase of 150 K in the transition temperature from the monoclinic ($P2_1/n$) to the orthorhombic (Pcnb) WO_3 phase. The monoclinic WO_3 phase vanished abruptly over a temperature range of only 50 K, instead of 180 K in the case of the Al-free support (Fig. 5a). As a consequence, in Al-SBA-15 (Si/Al ¼ 10) the orthorhombic phase which disappeared also at 830 K, existed over a narrower temperature range (730e830 K) than in the Al-free support (600e830 K). In contrast to the monoclinic and orthorhombic phases, the tetragonal WO_3 (P4/ncc) and the $WO_{2.92}$ (P2/c) phases were present in the same temperature range in SBA-15 and Al-SBA-15 (Si/Al ¼ 10). Finally, above 870 K, a small amount of WO_2 phase ($P2_1/c$, ICDD: 86-134) [40] appeared in Al-SBA-15 (Si/Al ¼ 10) which was not observed in the Al-free support.

The amount of each tungsten oxide phase in Al-SBA-15 (Si/Al ¼ 10) as a function of the reduction temperature was presented in the Fig. 5d. The complete reduction sequence was: WO_3 ($P2_1/n$) WO_3 (Pcnb) WO_3 (P4/ncc) $WO_{2.92}$ (P2/c) WO_2 ($P2_1/c$). After reduction at 885 K for 70 min the phases observed were WO_3 (P4/ncc), $WO_{2.92}$ (P2/c), and WO_2 ($P2_1/c$) (Fig. 5f). Compared to the Al-free sample, in which the amount of reduced phases remained constant all along the reduction treatment, WO_2 was progressively formed at the expense of $WO_{2.92}$ in the case of WO_3/Al-SBA-15 (Si/Al ¼ 10). After 70 min the sample contained 39, 41 and 20 wt.% of WO_3 (P4/ncc), $WO_{2.92}$ (P2/c), and WO_2 ($P2_1/c$), respectively.

This in situ XRD study also revealed that the tungsten carbide species not observed in this experiment are therefore formed between 885 K and 973 K.

3.7. Transmission electron microscopy

Representative transmission electron microscopy images of SBA-15 based materials are shown in Fig. 6. The image of the pure SBA-15 support (Fig. 6a) shows well-ordered channels characteristic of the 2-D hexagonal (P6mm) mesostructure, with clear and dark lines corresponding to the pores (channel core) and the pore channel walls, respectively. The average thickness of the wall is ca. 3e4 nm, and the pore diameter around 7-8 nm, in good agreement

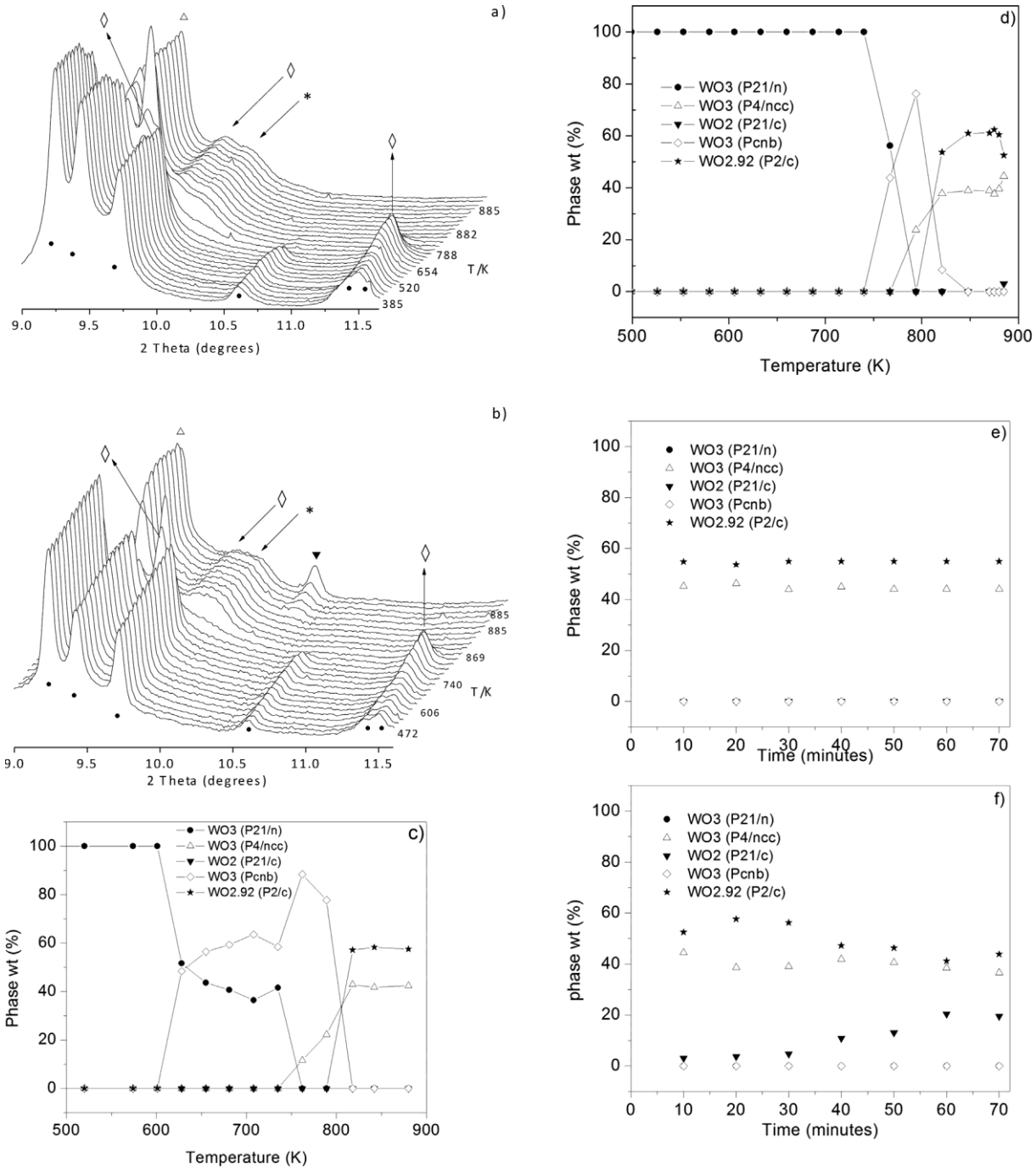

Fig. 5. In situ XRD patterns during reduction of: (a) WO_3/SBA-15 and (b) WO_3/Al-SBA-15 (Si/Al ¼ 10); evolution of the crystallographic phases quantified by the Rietveld method during the carburization process of the WO_3 monoclinic phase ($P2_1/n$) supported on SBA-15 (c) and Al-SBA-15 (Si/Al ¼ 10) (d) and evolution of the tungsten oxide phases at 885 K for 70 min of reduction on supports SBA-15 (e) and Al-SBA-15 (Si/Al ¼ 10) (f).

with the determinations from the N_2 adsorption tests. Al-containing samples (Al-SBA-15) also presented the same morphology (images not shown), preserving the ordered mesoporosity, which has also been ascertained by low-angle XRD.

Fig. 6b and c presents TEM images of WO_3/SBA-15 and WO_3/Al-SBA-15 (Si/Al ¼ 10), respectively. Both materials presented the mesoporous channel structure characteristic of SBA-15. These figures show the effect on the distribution of tungsten oxide species by the presence of aluminum in the SBA-15 substrate. In the WO_3/SBA-15 sample (Fig. 6b), tungsten oxide particles of about 100 nm can be noticed, whereas the tungsten oxide particles seem to be better distributed in the WO_3/Al-SBA-15 (Si/Al ¼ 10) material and no large particles of WO_3 were observed as in the previous case (Fig. 6c). WO_3/Al-SBA-15 (Si/Al ¼ 10) sample shows a great decrease in the pore size (from 9.42 nm to 7.59 nm) compared to the W-free sample which is mirrored in an increase of wall thickness, suggesting a preferential formation of WO_3 particles in the channels of the mesoporous structure. Similarly, TEM images of sample WO_3/Al-SBA-15 (Si/Al ¼ 2) show SBA-15 particles where contrasted areas are predominant (Fig. 6d). Since WO_x would present higher contrast than Al, these dark areas can be ascribed to WO_3 particles well distributed along the Al-SBA-15 support. Further, the absence

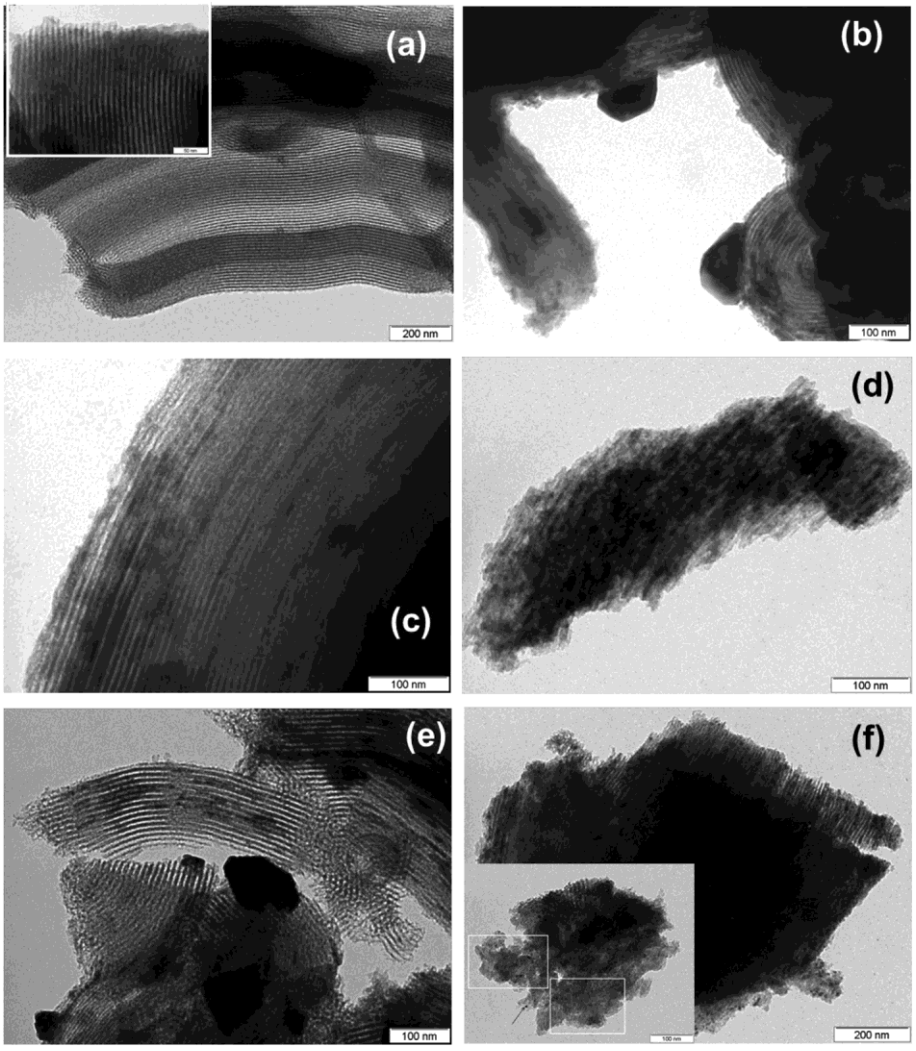

Fig. 6. Transmission electron microscopy images of: (a) SBA-15 and (b) WO_3/SBA-15; (c) WO_3/Al-SBA-15 (Si/Al ¼ 10); (d) WO_3/Al-SBA-15 (Si/Al ¼ 2); (e) W_2C/SBA-15 (f) W_2C/Al-SBA-15 (Si/Al ¼ 10).

of isolated or large WO_3 particles indicates that their formation may be produced into the channels of the mesoporous structure matching with our previous results obtained by PXRD, N_2 adsorption/desorption and Raman spectroscopy.

The mesoporous structure was also preserved in the W_2C-SBA-15 sample (Fig. 6e), consistently with the low angle XRD results. Compared to SBA-15 (Fig. 6a) and also more slightly to WO_3/SBA-15 (Fig. 6b), darker areas appear within the channel network, presumably due to carbides that are incorporated into the pore cavities of the mesostructure. In addition, dark particles of about 100 nm not dispersed into the mesostructure are observed. The carbide particles are better distributed in the W_2C/Al-SBA-15 (Si/Al¼10) as shown in Fig. 6f. However, small particles of less than 10 nm can be distinguished on the support in this case (Fig. 6f and inset). These particles could be due to migration of some WO_x particles from the inner pores to the outer part of the support due to the high temperatures during the TPC treatment.

Fig. 7 shows an overview of the synthesized W_2C/SBA-15 sample at low and high magnifications obtained by HRTEM. At lower magnification (upper left-hand panel) it can be seen that the ordered mesoporous structure of SBA-15 has been preserved after the TPC process. The areas marked as A and B are magnified in separate panels. In these, larger W_2C particles can be observed outside the porous channels of the mesoporous silica, while smaller particles are also present within the channels. This is more clearly presented in the extending area B (bottom right-hand side picture).

The microscopy results can give an insight on the reducibility behavior found by in situ XRD. A possible explanation to this could be related to both the interaction degree of the WO_3 P21/n phase and the size of particles in the different supports.

On the one hand, it has been demonstrated that WO_3 particles are less aggregated in Al-SBA-15 as a consequence of their higher interaction with the support. Moreover WO_3 particles are embedded in the channels. These effects lead to a higher stability of the WO_3 (P21/n) phase which is transformed into WO_3 (Pcbn) phase at a temperature 150 K higher than that found on pure silica support under reducing atmosphere.

On the other hand, only in the case of WO_3/Al-SBA-15 (Si/Al ¼ 10) the reduction process leads to the formation of about 20 wt.% WO_2 after 70 min of treatment at 885 K. This may be due to a larger amount of small tungsten oxide particles highly accessible because of their migration outside the mesoporous channels in the aluminum-containing support and thus easily reduced. The results above suggest that the reduction of WO_3 to WO_2 depends on the location and the interaction of the particles within the channels of the mesoporous support as well as of the size of the particles. Yang

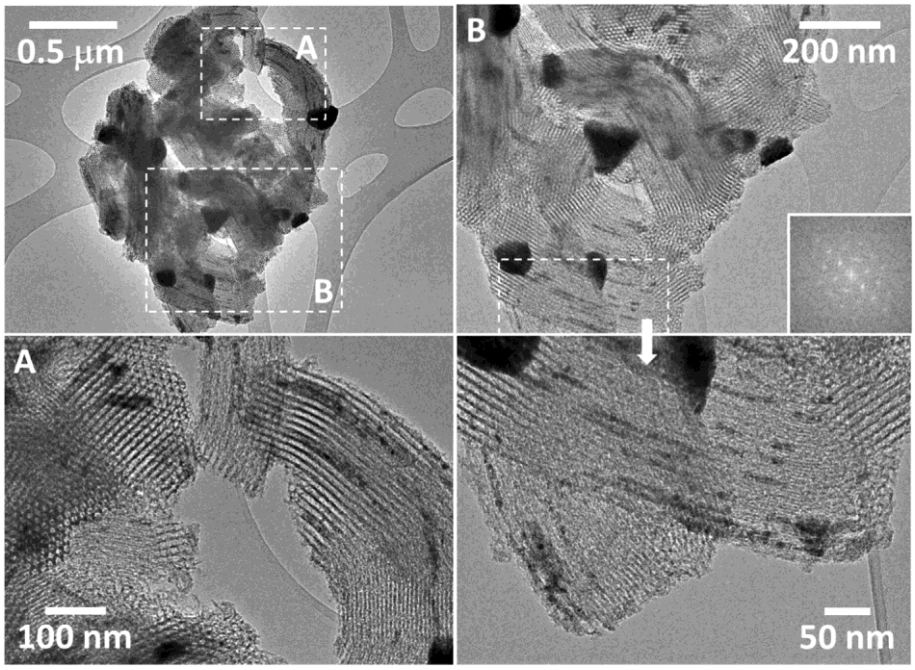

Fig. 7. High resolution TEM of W_2C/SBA-15 sample.

et al. [41] observed that reduction of W-doped SBA-15 samples depends on the content and dispersion of WO_3 and A. de Lucas et al. [42] found that the reducibility of WO_3/HZSM5 increased with decrease in dispersion. These facts can be attributed to higher oxide-support interaction for samples with higher dispersion. In addition, according to M'Boungou et al. [30] interaction between WO_3 and the support is weaker in WO_3-SiO_2 than in WO_3-Al_2O_3, thus WO_3 is more easily reduced in the former case. In our study, the supported tungsten oxide species are more strongly interacting and embedded in the Al-SBA-15 support, a conclusion indeed reinforced by XRD, Raman and TEM results. These features cause an upward shift in the reduction temperature of the tungsten oxides species. However, small and highly accessible particles only present in Al-SBA-15 (Si/Al ¼ 10) can explain the formation of a slight amount of WO_2 phase.

4. Conclusions

A series of Al-SBA-15 materials with molar ratios Si/Al of 2 and 10 have been prepared by the pH-adjusting method, as well as SBA-15 reference material. ^{27}Al NMR studies have revealed that the aluminum species are incorporated into the framework of the mesoporous silica SBA-15. However, the sample with higher amount of Al (Si/Al ¼ 2) presented segregated Al species. Aqueous impregnation of SBA-15 materials with the tungsten precursor did not lead to the destruction of the ordered mesoporous structure as demonstrated by the presence of XRD patterns at low scattering angles which indicates that the long-range ordering was not damaged. Tungsten carbide (W_2C) has been obtained by carburization of WO_3/SBA-15 and WO_3/Al-SBA-15 (Si/Al ¼ 10 and Si/Al ¼ 2) materials. The introduction of aluminum in the SBA-15 support favored the formation of smaller WO_3 and W_2C particles and greatly enhanced their distribution on the support after the calcination and carburization steps. This enhanced distribution was revealed by Raman analysis. The mesoporous structure of the silica materials was preserved in all the samples as ascertained by XRD, TEM and HRTEM. The in situ XRD analysis of the tungsten oxide reduction process revealed that the presence of aluminum species in the SBA-15 framework raised the reduction temperature range of the tungsten oxide species, due to interaction of W species with the support.

Acknowledgements

R.J. Chimentao and M.G. Alvarez gratefully acknowledges the Universitat Rovira i Virgili (URV) and Spanish Ministry of Science and Technology for the financial support for the Juan de la Cierva program (JCI-2010-07328) and grant CTQ2012-35789 and CTQ2006-08196 (255-EST-FPI). We also would like to acknowledge European Synchrotron Radiation Facility (ESRF) for the user facil- ities for the in-situ XRD measurements. We also would like to acknowledge Dr. German Castro, Dr. Iván da Silva and Dr. Alvaro Muñoz for the technical support offered at the ESRF (experiment MA-1525). J.L. and F.M. are grateful to the ICREA Academia program.

References

[1] C.T. Kresge, M.E. Leonowicz, W.J. Roth, J.C. Vartuli, J.S. Beck, Nature 359 (1992) 710e712.
[2] D.Y. Zhao, J. Feng, Q. Huo, N. Melosh, G.H. Fredrickson, B.F. Chmelka, G.D. Stucky, Science 279 (1998) 548e552.
[3] D.Y. Zhao, Q. Huo, J. Feng, B.F. Chmelka, G.D. Stucky, J. Am. Chem. Soc. 120 (1998) 6024e6036.
[4] J.P. Palmquist, Zs. Czigany, M. Odén, J. Neidhart, L. Hultman, U. Jansson, Thin Solid Films 444 (2003) 29e37.
[5] L. Volpe, M. Boudart, J. Solid State Chem. 59 (1985) 348e356.
[6] P.D. Costa, C. Potvin, J. Mol. Catal. A: Chem. 184 (2002) 323e333.
[7] M.K. Neylon, S. Choi, Appl. Catal., A 183 (1999) 253e263.
[8] A.P.E. York, J.B. Claridge, Chem. Commun. (1997) 39e40.
[9] J.S. Lee, L. Volpe, F.H. Ribeiro, M. Boudart, J. Catal. 112 (1988) 44e53.
[10] A.A. Voevodin, J.P. O'Neill, J.S. Zabinski, Thin Solid Films 342 (1999) 194e200.
[11] Y. Wang, Q. Chen, W. Yang, Z. Xie, W. Xu, D. Huang, Appl. Catal., A 250 (2003) 25e37.
[12] J.A. Horsley, I.E. Wachs, J.M. Brown, G.H. Via, F.D. Hardcastle, J. Phys. Chem. 91 (1987) 4014e4020.
[13] G. Leclercq, M. Kamal, J.M. Giraudon, P. Devassine, L. Feigenbaum, L. Leclercq, A. Frennet, J.M. Bastin, A. Lofberg, S. Decker, M. Dufour, J. Catal. 158 (1996) 142e169.
[14] L. Hu, S. Ji, T. Xiao, C. Guo, P. Wu, P. Nie, J. Phys. Chem. B 111 (2007) 3599e3608.

[15] S. Natesakhawat, R.B. Watson, X. Wang, U.S. Ozkan, J. Catal. 234 (2005) 496e508.
[16] J.G. Seo, M.H. Youn, I.K. Song, Int. J. Hydrogen Energy 34 (2009) 1809e1817.
[17] J.G. Seo, M.H. Youn, H.I. Lee, J.J. Kim, E. Yang, J.S. Chung, Chem. Eng. J. 141 (2008) 298e304.
[18] H. Devianto, Z.L. Li, P. Yoon, J. Han, S.W. Nam, T.H. Lim, H.I. Lee, Int. J. Hydrogen Energy 35 (7) (2010) 2591e2596.
[19] S.M. Riseman, F.E. Massoth, G. Murali Dhar, E.M. Eyring, J. Phys. Chem. B 86 (1982) 1760e1763.
[20] A. Corma, Chem. Rev. 97 (1997) 2373e2419.
[21] A. Corma, B.W. Wojciechowski, Catal. Rev.dSci. Eng. 27 (1985) 29e150.
[22] S. Wu, Y. Han, Y.C. Zou, J.W. Song, L. Zhao, Y. Di, S.Z. Liu, F.S. Xiao, Chem. Mater. 16 (2004) 486e492.
[23] L. Hu, S. Ji, Z. Jiang, H. Song, P. Wu, Q. Liu, J. Phys. Chem. C 111 (2007) 15173e15184.
[24] H.M. Kao, C.C. Ting, S.W. Chao, J. Mol. Catal. A 235 (2005) 200e208.
[25] Y.H. Yue, A. Gédéon, J.L. Bonardet, J.B. d'Espinose, N. Melosh, J. Fraissard, Stud. Surf. Sci. Catal. 129 (2000) 209e218.
[26] A.P. Legrand, The Surface Properties of Silicas, John Wiley & Sons Ltd., 1997, p. 2.
[27] G. Calleja, J. Aguado, A. Carrero, J. Moreno, Appl. Catal., A 316 (2007) 22e31.
[28] R. . van Grieken, J.M. Escola, J. Moreno, R. Rodríguez, Chem. Eng. J. 155 (2009) 442e450.
[29] E. Iglesia, D.G. Barton, S.L. Soled, S. Miseo, J.E. Baumgartner, W.E. Gates, G.A. Fuentes, G.D. Meitzner, Stud. Surf. Sci. Catal. 101 (1996) 533.
[30] J.S. M'Boungou, L. Hilaire, G. Maire, F. Garin, Catal. Lett. 10 (1991) 401e402.
[31] G.M. Kumaran, S. Garg, K. Soni, M. Kumar, J.K. Gupta, L.D. Sharma, K.S.R. Rao, G.M. Dhar, Microporous Mesoporous Mater 114 (2008) 103e109.
[32] N. Nakamoto, Infrared and Raman Spectra of Inorganic and Coordination Compounds, third ed., Wiley, New York, 1978.
[33] C. Catalini, H.T. Sun, M. Faccio, M. Pelini, S. Santucci, L. Lozzi, M. Passacantando, Sens. Actuators, B 31 (1996) 81e87.
[34] A. Kuzmin, J. Purans, E. Cazzanelli, C. Vinegoni, G. Mariotto, J. Appl. Phys. 84 (10) (1998) 5515e5524.
[35] W.D. Schubert, Int. J. Refract. Met. Hard Mater 9 (3) (1990) 178e191.
[36] P.M. Woodward, A.W. Sleight, T. Vogt, J. Phys. Chem. Solids 56 (1995) 1305e1315.
[37] T. Vogt, P.M. Woodward, B.A. Hunter, J. Solid State Chem. 144 (1999) 209e215.
[38] K.R. Locherer, I.P. Swainson, E.K.H. Salje, J. Phys.: Condens. Matter 11 (1999) 4143e4156.
[39] M.R. Sundberg, Acta Crystallogr. 32 (1976) 2144e2149.
[40] A.A. Bolzan, B.J. Kennedy, C.J. Howard, Aust. J. Chem. 48 (1995) 1473e1477.
[41] X.L. Yang, W.L. Dai, R. Gao, K. Fan, J. Catal. 249 (2007) 278e288.
[42] A. de Lucas, J.L. Valverde, P. Cañizares, L. Rodriguez, Appl. Catal., A 172 (1998) 165e176.